Heat and Mass Transfer
https://doi.org/10.1007/s00231-024-03495-8

RESEARCH

A novel investigation on single-loop pulsating heat pipe filling with hybrid nanofluids: numerical and experimental

Prem shanker yadav[1,2] · Jitendra sharma[1] · Mohd Hussain[1] · Imran ahmed Khan[1] · Kartik Goyal[1] · Samer Fikry Ahmed[3]

Received: 31 January 2024 / Accepted: 1 July 2024

Abstract
Pulsating heat pipes (PHPs) employ to multiphase heat transfer between condensers and evaporators. The efficacy of PHP is predominantly contingent upon the thermos-physical property exhibited by its working fluid. The exergy analysis of evaporator, adiabatic and condenser system were performed to evaluate the efficiency and sustainability of energy conversion processes, it was also seen that exergy loss of condenser was 1.01% higher than evaporator. Further, 2-D numerical simulation of a cryogenic pulsating heat pipe (CPHP) was conducted and also numerical and experimental simulation was conducted, where simulation results agreed with experimental results with 10% similarity. The simulation employs the volume of fluid (VOF) model to capture the dynamics of two-phase liquid–vapor flow within the CPHP employing liquid acetone – Al_2O_3 as the working fluid. The diameter of the single turn is systematically varied, ranging from 1 mm to 2.5 mm, while maintaining the filling ratio (FR) within the range of 25% to 75%. The evaporator temperature is adjusted within the span of 85 K to 115 K. The PHP exhibited best thermal performance at inner diameter of 2 mm among (1, 1.5, 2, 2.5 mm) and filling ratio of 55% among (25%, 45%, 55%, 65% and 75%).

Abbreviations

PHP	Pulsating Heat Pipe
CLPHP	Closed loop pulsating heat pipe
Al_2O_3	Aluminum oxide
BP	Boiling point
LHv	Latent heat of vaporization
D	Diameter
ρ_l	Density of liquid
ρ_v	Density of vapor
µm	Micro - meter
d_{crit}	Critical diameter
T_{max}	Maximum Temperature
Cp	Specific heat capacity
$T_{e,o}$	Temperature of working fluid exiting evaporator
σ	Boltzman constant
CFD	Computational Fluid Dynamics
d	Internal diameter
σ	Surface Tension
FR	Filling ratio
g/s	gram/second
mm	millimeter
MPa	Mega Pascal
nm	Nano - meter
VOF	Volume of fluid
Te	Evaporator Temperature
Tsat	Saturated Temperature
Te,i	Temperature of working fluid before entering evaporator
Tc,i	Temperature of working fluid before entering condenser
ε	Emissivity
Evap	Evaporator

✉ Prem shanker yadav
prem0jss@gmail.com

[1] Department of Mechanical Engineering, JSS Academy of Technical Education, Noida, India

[2] Department of Mechanical Engineering, Delhi Technological University, Delhi, India

[3] Mechanical and Industrial Engineering Department, College of Engineering, Qatar University, Doha, Qatar

1 Introduction

The Pulsating Heat Pipe (PHP), a passive heat transmission system, has been utilized for approximately 30 years. In regards to its structure, the PHP can be described as a hollow and winding pipe. Khandekar and Groll [1] is credited with the development of these devices, which exhibit tremendous

Published online: 10 July 2024

potential in various applications such as solar energy utilization, waste heat recovery, aircraft thermal management, and electronics cooling as shown in Fig. 1 [2]. PHPs are passive cooling systems that operate with two-phase flow, providing rapid heat transfer. They consist of 3—sections: the adiabatic, evaporator section and the condenser. The condenser as well as evaporator parts are thermally connected to a cold sink and a heat source respectively, using thermal anchors. Capillary tubing is employed to connect the condenser and evaporator part, these are bent back and forth repeatedly. There are three primary types of PHPs: Closed-loop with a check valve, Closed Loop, and Closed-ended PHPs [3]. In a CLPHP, a slug flow pattern is observed, characterized by the presence of vapor and liquid slugs, as depicted in Fig. 1. As vapor plugs move towards the condenser section, they undergo a reduction in volume caused by re-condensation and temperature influences, with certain vapor bubbles fully transitioning into the liquid phase. Boiling in the evaporator region results in the growth of existing vapor bubbles and the formation of new ones. These expansions and contractions of the two-phase fluid generate pressure fluctuations necessary for driving the flow. Fluids characterized by a high $(dP/dT)_{sat}$ are considered preferable due to the substantial pressure shift observed in vapor bubbles with only a slight temperature adjustment at saturation levels [4].

However, the selection of the working fluid plays a crucial role in determining the performance of a PHP. Selecting a suitable working fluid that meets the operating temperature range, heat transfer requirements, and compatibility with the materials used in the PHP can be a challenge. Furthermore, the availability and cost of the chosen fluid can also impact

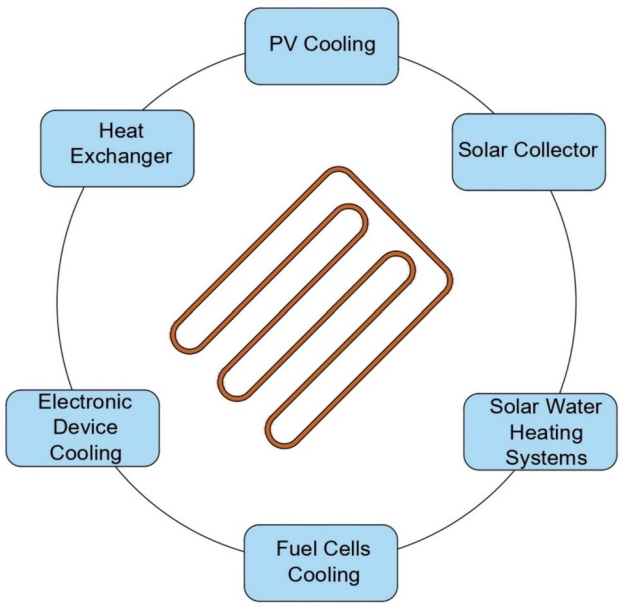

Fig. 1 Applications of PHP

the practicality of PHP implementation [5, 6]. Further, Zhang et al. [7] examined that it is simpler to start up a working fluid with low surface tension, low dynamic viscosity and high thermal conductivity. Acetone's low latent heat and low surface tension make it simpler to dry out than other working fluids [8]. The increased flow speed of nanofluids in PHP was noted by Zhang et al. [9]. PHP can typically start and run between 20 and 80% of the filling ratio. While, high filling ratio prevents the production of vapor plugs and impedes flow, whereas a low filling ratio makes it difficult to cause oscillation of the operational fluid [10, 11].

The sensible heat also plays a crucial role in dissipating a significant amount of heat as the heat flux supplied to the evaporation section is minimal. In such cases, where the heat transfer rate is relatively small, the majority of heat transfer occurs through the sensible heat mechanism. Further, the ability to maintain the oscillation motion at a lower required heat flux is crucial for the performance and effectiveness of the PHP. Therefore, opting for a working fluid with lower viscosity can contribute to enhancing the overall heat transfer efficiency of the system [12, 13]. The results of Qu et al. [14] demonstrated that among the tested working fluids such as acetone, methanol and water, acetone exhibited the best heat transfer performance in the PHP system. Despite the low heat flux input, acetone proved to be the most effective choice in terms of facilitating heat transfer within the PHP. The major portion of heat transfer is accomplished through the sensible heat of the liquid, while the latent heat of vaporization plays a secondary role [15]. Liang et al. [16] investigated the thermal performance of a cryogenic PHP and specifically examined the influence of condenser temperature and filling ratio. The findings demonstrated that a lower filling ratio led to a dry-out phenomenon occurring at lower heat inputs. Zhang et al. [17] conducted experiments taking FC-72, ethanol, and water as working fluid, and found that the best fill ratio for all three fluids was around 70%, with lower and higher fill ratios resulting in lower thermal performance. At this fill ratio, the mean temperatures in the heating section were lowest and the thermal performance was highest. In an experimental study conducted by Saha et al. [18], two open PHPs were examined. The results of the experiment indicated that the PHP with a 0.9 mm inner diameter exhibited superior performance compared to the PHP with a 1.5 mm inner diameter. It is worth noting that the physical properties of the working fluid can influence the impact of the inner diameter on the PHP's performance, as highlighted by Rittidech et al. [3]. Specifically, it was observed that a larger inner diameter resulted in improved heat transfer performance for R123, while it led to poorer performance for ethanol. Hybrid nanofluids, which are a combination of base fluids and nanoparticles, are being

increasingly explored for use in PHPs due to their potential to enhance thermal performance. The addition of nanoparticles to the base fluid in PHPs can offer several benefits such as improved thermal conductivity and heat transfer coefficient, reduced thermal resistance and controlled fluid flow. However, there are some challenges in utilization of nanofluids such as particle agglomeration, difficulty in nanoparticle dispersion [19–21].

Karthikeyan et al. [22] explored the use of nano-fluids, specifically Ag-deionized water and Cu-deionized water, within the range of heating power from 50 to 240 W. Their findings indicated a noteworthy 33.3% increase in the heat transfer capacity of the PHP when employing nano-fluids compared to the utilization of pure deionized water. Ji et al. [23] scrutinized the heat transfer characteristics of the PHP utilizing Al_2O_3-water with varying particle sizes (80 nm, 50 nm, 22 µm, and 2.2 µm). Their observations revealed that the initiation power of the PHP decreased proportionally with the reduction in particle size. Tanshen et al. [24] examined the thermal resistance of the PHP employing nano-fluids containing multi-walled carbon nanotubes (MWCNT) across four mass ratios (0.2, 0.3, 0.05, and 0.1 wt%). The outcomes they obtained suggested that the PHP attained its peak inner evaporation pressure, and concurrently, the thermal resistance of the PHP reached its minimum at a mass ratio of 0.2 wt%. Changes in boiling performance in heat pipes directly affect the surface properties, as indicated in relevant literature sources [25–27]. The presence of nanoparticles in the base fluid does not significantly increase the thermal conductivity of the working fluid. However, the oscillatory movement of particles within the working fluids may offer additional enhancement to the thermal performance of the CLPHP.

From this comprehensive review, it becomes evident that there are two significant research gaps noticed.

(a) No previous studies have explored the effects of acetone- Al2O3 on the exergy and sustainability. These analyses serve as contemporary tools for evaluating the effectiveness of systems, offering valuable insights and conclusions.
(b) Additionally, there is a notable absence of research investigating the optimum diameter and filling ratio for acetone- Al2O3 fluid to get maximum performance.

The first section of the study evaluates the thermodynamic analysis and sustainability analysis. The subsequent section outlines the governing equations and computational techniques utilized for the CFD analysis at various diameter to analyze the flow characteristics within a PHP. Getting optimum diameter, filling ratio was varied to get the enhanced performance of PHP.

2 Experimental setup and description of operation of a PHP

The internal pipe diameter, represented by the Bond dimensionless number ($B_0 = (\rho_l - \rho_v)gd/\sigma$) plays a crucial role in characterizing phase separation within the PHP device [28]. In Taylor bubble-rising experiments involving water boiling in vertical tubes, it has been observed that when the bond number is less than 2, the vapor bubble and the wall film maintain radial symmetry due to the dominant influence of surface tension over gravitational force [29]. PHPs exhibit remarkable operational stability across various orientations, allowing them to function successfully. The stability is attributed to the diverse flow regimes that can be observed in a PHP, as depicted in Fig. 2. Under low heat loads, the vapor phase diffuses into the liquid phase, leaving the nucleation sites on the walls. As evaporation intensifies, the number of small and micro-bubbles increases, with the smaller bubbles migrating towards the core region. These bubbles engage in interactions with each other and frequently merge, forming

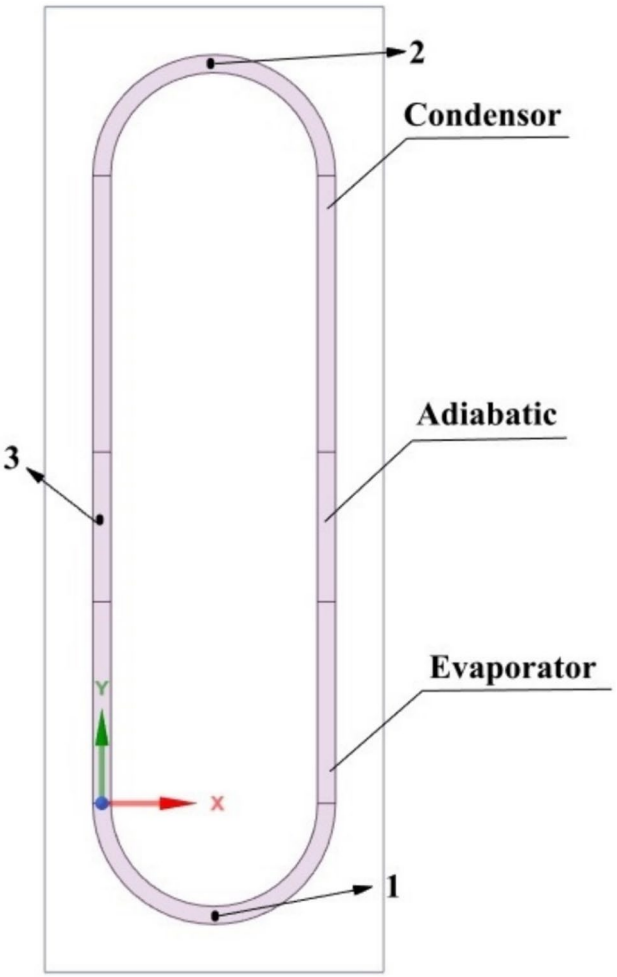

Fig. 2 Single loop pulsating heat pipe model

larger bubbles. With a continued rise in heat load, the dimensions of these aggregations of bubbles progressively enlarge, eventually resulting in the separation of the mixed-phase fluid into alternating liquid segments known as slugs and vapor segments referred to as plugs. When the capillary length is larger than internal diameter of the pipe, the aforementioned formations spread radially and occupy the pipe's core space. With increased energy input, the phase change intensifies the turbulence and movement, making the segments unstable. In such unstable conditions, the structures have a tendency to break down into chaotic swirls, eventually forming small droplets. This phenomenon gives rise to a flow regime with enhanced heat transmission capabilities, known as annular flow [30, 31]. Within such a regime, the flow field within The PHP can be segmented into two clearly defined regions. The core region comprises a liquid film wall layer along with a mixture of dispersed liquid and vapor phase. Notably, significant interactions occur between the wall and core regions in this mode. At extremely elevated levels of core flux, droplets carried along in the core flow have the potential to condense into liquid masses, akin to vapor conglomerates. This condensation process contributes to pressure instability [32]. PHPs leverage these instabilities to generate a unique mixed-phase flow, setting them apart from conventional heat pipes. The fluid within the PHP is propelled along the serpentine tube by a pressure gradient, which arises due to local variations in the rates of condensation and evaporation. Pulsation is initiated by the shifting direction of chains of slugs and plugs due to an imbalance in the total force [33]. The areas of a PHP have varying velocities due to expansion from liquid evaporation and contraction from vapor condensation, respectively. These localized motion fields have the potential to interact with each other as waves and change in strength as a result.

A region exhibiting alike flow velocity and direction can form if certain locations are connected as the heat load rises. The circular flow regime, which enhances heat capacity and can withstand a large heat load, tends to emerge in the single-directional field [34]. The robust interactions of the wall boundary layer also contribute to heat transmission. A bubble traveling through the channel exhibits an unbalanced head and a less orderly tail. The bubble having thin liquid film is disrupted by the turbulence created in the wake zone, leading to a local increase in the heat transfer coefficient. This enhanced convection is primarily responsible for thermal transfer that surpasses conduction within the solid wall by orders of magnitude [35].

Figure 3 illustrates the experimental apparatus employed in the present study. The condensation, adiabatic and evaporation sections comprise a length of 50 mm each. The pulsating heat pipe is constructed using quartz glass having 6 mm outer diameter. For visualization purposes, it has an inner diameter of 3.8 mm. The current PHP has a sufficiently small inner diameter, allowing the working fluid, water, to spontaneously disperse as liquid–vapor slugs. It is oriented vertically, with the bottom-heating pattern. A heating wire, measuring 0.4 mm in diameter, is wrapped around the surface of the evaporation section. Additionally, a water cooler is submerged in the condensation area. The water cooler's inlet temperature is maintained at 25 °C, while a fix flow rate of 4.69 g/s is prescribed. The current PHPs undergo evacuation to 0.079 MPa using a vacuum pump. Subsequently, water is introduced into the PHPs through the injection entrance, as illustrated in Fig. 3. In this study, different filling ratios of 30%, 40%, 50%, and 60% are employed for the PHPs. Furthermore, the heating power can be adjusted within the range of 5W to 40W by modifying the output voltage. The experimental setup depicted in Fig. 3 includes six T-type thermocouples positioned on the outer wall of the PHP. These thermocouples are specifically labeled as Te_1 and Te_2 for the evaporation section, Ta_1 and Ta_2 for the adiabatic section, and Tc_1 and Tc_2 for the condensation section. Real-time temperature data is collected using an agilent 34970A data acquisition system, which is connected to a computer and programmed to scan the temperatures at intervals of 5 s. This continuous data acquisition enables the determination of the experimental thermal resistance (Rex) of the PHP. The average temperatures of the evaporation and condensation sections are denoted as T_e and T_c, respectively. The input heating power is represented by Q in the equation $Rex = \frac{(T_e - T_c)}{Q}$.

The working fluids having minimum latent heat of vaporization, lower boiling point and liquid specific heat can begin pulsating very readily inside the pulsating heat pipe, however, they are low energy carrier. Further, low dynamic viscosity fluids experience lesser flow resistance resulting strong pulsating effects due to high flow rate [33]. Table 1 shows the thermos-physical properties of water, acetone and acetone-Al_2O_3 and it was observed that acetone-Al2O3 consist of low dynamic viscosity, liquid specific heat and latent heat of vaporization and that improves pulsating effects in PHPs. The diameter is varied from 1 mm to 2.5 mm based on bond no which shows the critical diameter 2.1 mm. Further, investigation is performed order to get the optimum filling ratio which is considered from 25 to 75%.

Uncertainty analysis involves estimating the true value from the mean of repeated measurements. The errors observed in the test data primarily stem from the heating procedure and the subsequent recording of temperature data. For a given parameter, six experiments were conducted, and the average was used for error analysis. The uncertainty associated with the total thermal resistance of PHP can be estimated using Holman's square root rule as shown in Eq. 1 [36].

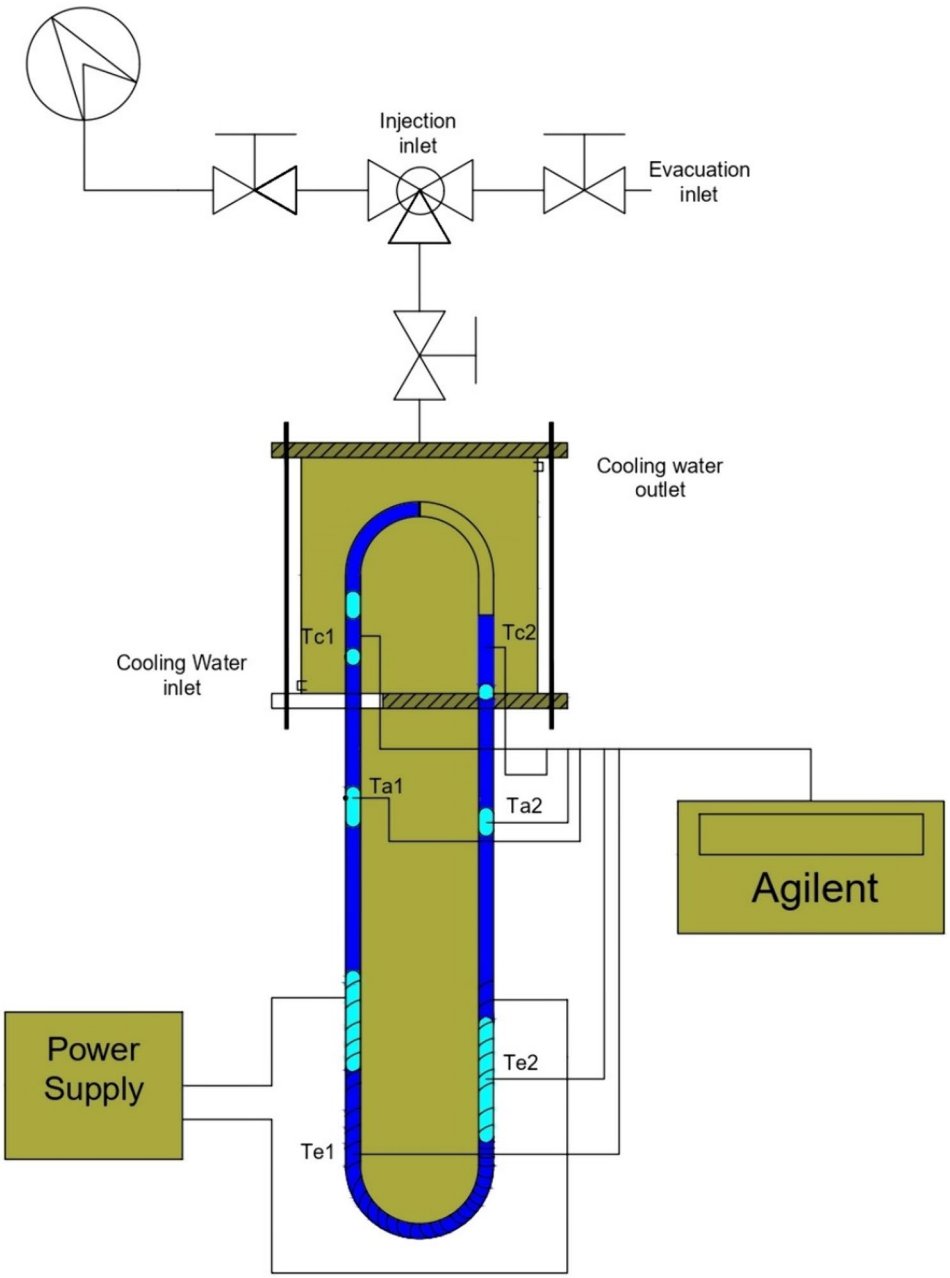

Fig. 3 Experimental set-up single loop PHP

$$U_E = \{[(\frac{\partial E}{\partial X_1})u_1]^2 + (\frac{\partial E}{\partial X_2})u_2]^2 + (\frac{\partial E}{\partial X_3})u_3]^2 + \ldots\ldots\ldots + (\frac{\partial E}{\partial X_n})u_n]^2\}^{1/2} \quad (1)$$

Here, E denote the fundamental variable impacting the other variables, $X_1,\ldots,Xn$. X corresponds to the quantities utilized during the experimental process, and $u_1,\ldots,u_n$

Table 1 Effect of Al_2O_3 on thermo-physical properties of working fluid

Working fluids	LHv (Hrg)	Surface Tension ($\sigma \times 10^3$) N/m	Boiling point (Ts ^{0}C)	Liquid density, ρ_l (kg/m^3 20^{0}c)	Thermal conductivity, λ_l (W/(Mk)) 20^{0}c	Liquid specific heat, C_{pl} (KJ/kgK) 20^{0}C	Dynamic viscosity ($\upsilon_l \times 10^3$) Pa.s 20^{0}C	$(dp/dt)^*_{sat}$ X 10^3 (Pa/K, 80^{0}C)	Ref.
Water	2257	72.8	100	998	0.599	4.18	1.01	1.92	[33]
Acetone	523	23.7	56.2	792	0.170	2.35	0.32	6.27	[33]
Acetone-Al_2O_3	516	24.8	-	798	0.206	2.32	0.28	-	Present

represent the uncertainties associated with these measurements. Consequently, the comprehensive uncertainty of the experimental findings can be described as following Eq. (2).

$$\frac{\Delta R}{R} = \sqrt{\left(\frac{\Delta(T_{ave,e} - T_{ave,c})}{Q_{in}}\right)^2} = \pm 1.96\% \tag{2}$$

The change in thermal resistance (ΔR), when considered, reveals that the maximum uncertainty in the overall heat input and thermal resistance in PHP falls well within the ± 1.96% range.

The total uncertainty value is ± 1.96%, which falls within the range reported by prior studies [37].

3 Exergy analysis

This is a thermodynamic approach employed to evaluate the quality or usefulness of energy within a system. It takes into account both the energy content and the thermodynamic irreversibility in the system [38]. In the case of a PHP, two-phase heat transfer passive device, it can be performing an exergy analysis to evaluate the efficiency and losses within the system. Here a single turn PHP with an adiabatic, evaporator, and a condenser section. The exergy balance equations for each section are as follows:

Evaporator section

The heat transfer in a PHP involves two main components: liquid slug flow and vapor flow. The exergy change in the evaporator section is given by Eq. 3 [3]:

$$\Delta Ex_E = mC_p[(Te, i - Te, o) - To \ln\left(\frac{Te, i}{Te, o}\right)\}] \tag{3}$$

The heat loss can be expressed as the sum of convective heat transfer and radiative heat transfer as in Eqs. 4 and 5 [39]

$$\Delta Ex_{e,1} = \Delta Ex_{co,1} + \Delta Ex_{ra,1} \tag{4}$$

$$\Delta Ex_{co,1} = hco \times As \times \Delta T \tag{5}$$

where, $\Delta Ex_{e,}$ $\Delta Ex_{e,l}$, $\Delta Ex_{co,l}$,, $\Delta Ex_{ra,l}$ are net exergy change across evaporator, exergy loss through evaporator, convective exergy loss and radiative exergy loss respectively.

Radiative heat transfer in a PHP evaporator occurs through thermal radiation between the evaporator surface and the surroundings. The radiative heat transfer rate can be estimated using the following Eq. 6 [39]

$$\Delta Ex_{ra,1} = \sigma \times \varepsilon \times As \times (T_{sf}^4 - T_{sr}^4) \tag{6}$$

Adiabatic section

Since the adiabatic section does not involve any heat transfer, the exergy change is only due to the fluid friction losses:

$$\Delta Ex\_adiabatic = W\_friction$$

where:

$\Delta Ex\_adiabatic$ is the change in exergy in the adiabatic section,

W_friction is the work done against fluid friction losses. It is assumed that the pressure drop is very less throughout the adiabatic section therefore the losses in adiabatic section is negligible.

Condenser section

Similar to the evaporator section, the exergy change in the condenser section can be expressed as per Eq. 7 [7]:

$$\Delta Ex_c = mC_p[(Tc, i - Tc, o) - To \ln\left(\frac{Tc, i}{Tc, o}\right)\}] \tag{7}$$

where:

The heat loss can be expressed as the sum of convective heat transfer and radiative heat transfer as in Eqs. 8 and 9 [9].

$$\Delta Ex_{c,1} = \Delta Ex_{co,1} + \Delta Ex_{ra,1} \tag{8}$$

$$\Delta Ex_{co,1} = hco \times Asc \times \Delta T \tag{9}$$

where, ΔEx_c $\Delta Ex_{c,1}$, $\Delta Ex_{co,1}$, $\Delta Ex_{ra,1}$ are net exergy change across condenser, exergy loss through condenser, convective exergy loss and radiative exergy loss respectively. Radiative heat transfer in a PHP evaporator occurs through thermal radiation between the evaporator surface and the surroundings. The radiative heat transfer rate can be estimated using the following Eq. 10 [40]

$$\Delta Ex_{ra,1} = \sigma \times \varepsilon \times Asc \times (T_{sf}^4 - T_{sr}^4) \tag{10}$$

The exergy efficiency of a PHP can be calculated by comparing the actual exergy transfer in the system to the maximum possible exergy transfer. The exergy efficiency $\eta_{\Delta E_X}$ is defined as the ratio of the actual exergy transfer to the maximum exergy transfer as given in Eq. 11 [39, 40]:

$$\eta_{\Delta E_x} = \frac{(Ex\_out - Ex\_in)}{Ex\_in\_\max} \tag{11}$$

Sustainability Assessment Sustainable development requires the resources to be used efficiently. Employing the exergy analysis method proves to be a valuable tool for optimizing advantages and utilizing resources efficiently. In this analysis, the SI method directly related to exergy efficiency $\eta_{\Delta E_x}$ is used to improve and contribute to the sustainable development as follows [41] as in Eq. 12:

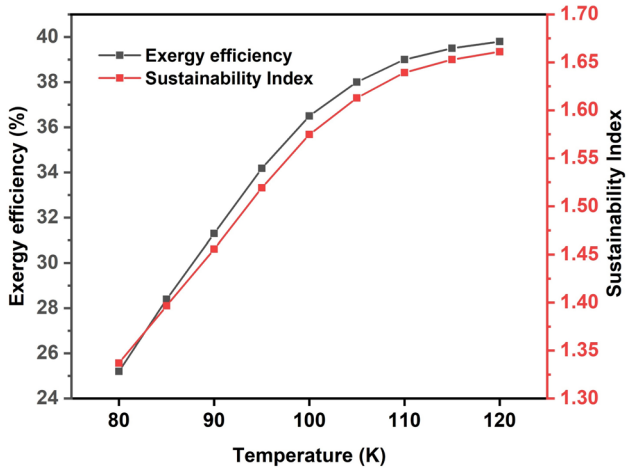

Fig. 4 Exergy efficiency and sustainability vs temperature

$$SA = \frac{1}{(1 - \eta_{\Delta EX})} \tag{12}$$

Figure 4 demonstrate the sustainability index and exergy efficiency in terms of reference temperature. It can be observed that exergy efficiency initially increased and further rate of increment got decrease. This is due to rise in exergy loss. In the given range of reference temperature, the exergy efficiency is highest at 120 K of temperature.

The sustainability index also showed the similar pattern of exergy efficiency and that confirms the resources can be utilized efficiently.

In the evaporator, as the reference temperature rises, the temperature difference between the working fluid and the surroundings also increases. This larger temperature gradient results in higher heat transfer irreversibilities and, consequently, higher exergy losses as shown in Fig. 5.

Similarly, in the condenser, a higher reference temperature means a higher temperature difference between the working fluid and the surroundings during heat rejection. This increased temperature gap results in greater irreversibilities and higher exergy losses.

4 Simulation and modeling

Figure 6 illustrates a 2-D physical model of a single loop PHP, where acetone – Al_2O_3 serves as the operating fluid. The PHP is positioned for bottom heating, and it has an overall length span of 57 mm. In order to ensure that the dominance of surface tension force over gravitational force is evident within the channel, which measures 1 mm, the calculation of the inner critical diameter of the PHP involves the use of the Bond number (Eq. 1, The inner diameter (D) of the CPHP must be smaller than the critical diameter (D_c) for proper functionality). Thus, the current CPHP model's inner diameter is set at 1 mm.

Fig. 5 Exergy loss vs reference temperature

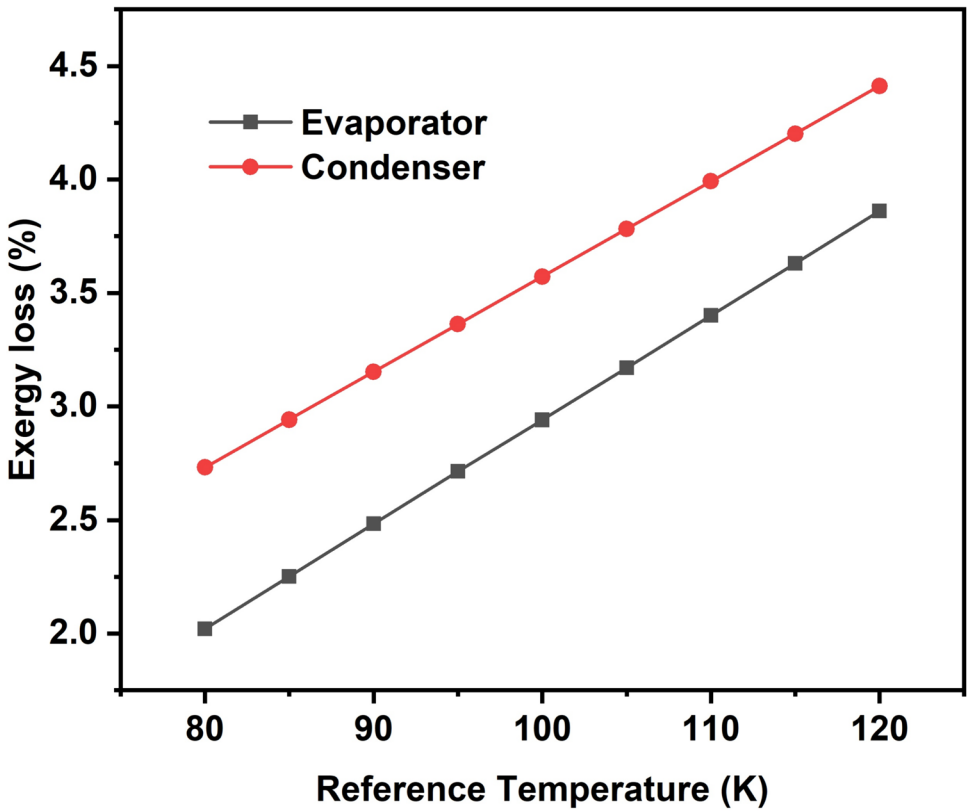

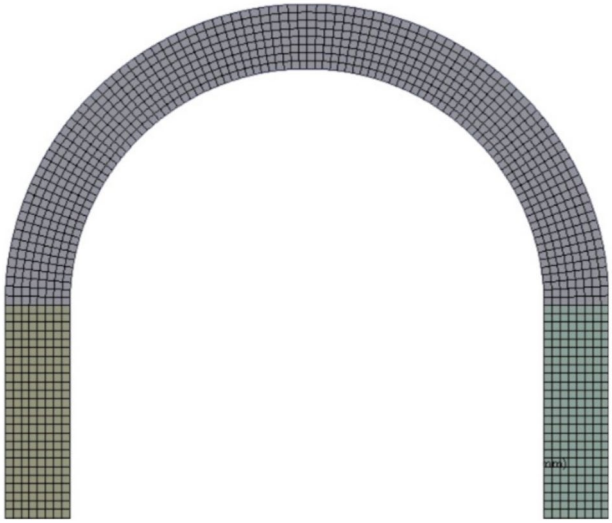

Fig. 6 A mesh structure adopted in a 2-D CPHP model

To accurately account for the surface tension effect, a quadrilateral mesh is favored over tetrahedral and triangular meshes [42]. Accordingly, quadrilateral structured mesh has been employed. Figure 6 illustrates the utilized quadrilateral mesh in the 2-D PHP model. The thickness of the first layer adjacent to the wall is set at 0.18 mm.

The flow dynamics in a PHP can be described as a two-phase gas-liquid flow regime. This regime is characterized by the presence of gas bubbles interspersed with liquid slugs [43]. The VOF approach enables the modeling of the two-phase flow by tracking the interface between the gas and liquid phases. The VOF approach ensures that the distinct gas and liquid phases within a PHP, characterized by bubbles and liquid slugs, are appropriately represented without mixing or overlapping. The variables are integrated for each introduced phase in the model, ensuring that the total sum of volume fractions for all phases within a computational cell equals unity. The properties and variables in a cell exhibit either two phase mixture or single phase and that relies on volume fraction values (Table 2).

Consider the fluid volume fraction in a cell, denoted as αq, representing the volume percentage of the fluid labeled as "qth.". There are three possible conditions: $\alpha q = 1$, $\alpha q = 0$ and $0 < \alpha q < 1$ are indicated as full cell, empty cell (for qth fluid) and interface between two fluids. Depending on the value of αq, appropriate variables and properties are assigned to every control volume within the domain. Further, it is postulated that phase transition transpires at the saturation temperature when transitioning between the vapor and liquid phases. Equation (13) represents mass conservation equation [44].

$$\frac{\partial(\alpha_v \rho_v)}{\partial t} + \nabla.(\alpha_v \rho_v \upsilon_v) = \dot{m}_{lv} - \dot{m}_{vl} \tag{13}$$

The interphase mass transfer is described as in Eqs. 14 and 15 [44].

Here, $T_l > T_{sat}$ (for evaporation)

$$\dot{m}_{lv} = r_{lv}.\alpha_l \rho_l \frac{(T_l - T_{sat})}{T_{sat}} \tag{14}$$

If, $T_{sat} > T_v$ (for condensation)

$$\dot{m}_{vl} = r_{vl}.\alpha_l \rho_l \frac{(T_l - T_{sat})}{T_{sat}} \tag{15}$$

where, r indicates relaxation factor,

The relaxation factor, denoted as 'r,' is set to a default value of 0.1 s-1 to ensure the interface temperature remains in proximity to the saturation temperature of the working fluid [45]. Throughout the domain, the momentum equation (Eq. 16) is computed, the momentum equation's outcome is influenced by the volume fractions of each phase [46].

$$\frac{\partial(\rho\vec{v})}{\partial t} + \nabla.(\rho\vec{v}\vec{v}) = -\nabla P + \nabla.[\mu(\nabla\vec{v} + \nabla\vec{v}^T)] + \rho\vec{g} + \vec{F}_{vol} \tag{16}$$

Surface tension emerges due to the cohesive forces among molecules present in the fluid. These surface forces become dominant, particularly in mini channels. The CSF model is employed for surface tension modelling in FLUENT. Incorporating surface tension into the VOF formulation introduces it as a source term in the momentum equation. The volume force acts on the surface are given by Eq. (17) [47].

$$F_{vol} = \sigma_{lv} \frac{\alpha_v \rho_v k_l \nabla\alpha_l + \alpha_l \rho_l k_v \nabla\alpha_v}{\frac{1}{2}(\rho_v + \rho_l)} \tag{17}$$

Table 2 Numerical simulation matrix

Items	Content	Items	Content
Multiphase model	VOF Implicit /Explicit	Volume Fraction	Geo-Reconstruct
Viscous model	k-epslion	Model	2D transient
Energy and Momentum and	Upwind second Order	Mesh	Quadrilateral
Pressure interpolation	PRESTO	First layer thickness	0.18 mm
Gravitational acceleration	-9.81 m/s 2, Y axis	Modeling of surface tension force	CSF

The curvature (k) is mathematically represented as follows: $k_l = \frac{\nabla \alpha_l}{\nabla \alpha_v}$, $k_v = \frac{\nabla \alpha_v}{\nabla \alpha_l}$.

Further, the Eq. (18) shows the energy equation contributed among phases [48]. Where, Sh exhibits the energy source due to phase change. It is acquired by multiplying the latent heat by the rate of mass transfer such as

$$S_h = -h_{LH}\, m_{lv} = h_{LH}\, \dot{m}_{vl}$$

$$\frac{\partial}{\partial t}(\rho E) + \nabla.(\vec{v}(\rho E + P)) = \nabla.(K.\nabla T + (\overline{\overline{\tau}}.\vec{v})) + S_h \tag{18}$$

The two terms of Eq. (18) in right side are the sum of energy transfer through viscous dissipation and conduction.

In Eq. (19), the temperature (T) and energy (E) are considered as mass-averaged variables in volume of fluid (VOF) model [47].

$$E = \frac{\alpha_v \rho_v E_v + \alpha_l \rho_l E_l}{\alpha_v \rho_v + \alpha_l \rho_l} \tag{19}$$

where, Ev and E_l are depends on specific heat of phases and shared temperature as in Eqs. 20 and 21.

$$E_v = C_{v,v}(T - T_{sat}) \tag{20}$$

$$E_l = C_{v,l}(T - T_{sat}) \tag{21}$$

The properties K, ρ and μ are common to all phases, as presented below:

$$K = \alpha_v K_V + \alpha_l K_l,\ \rho = \alpha_v \rho_v + \alpha_l \rho_l,\ \mu = \alpha_v \mu_v + \alpha_l \mu_l$$

5 Results and discussion

5.1 Validation of model and grid sensitivity test

The results of laboratory research on a PHP were compared with previous simulations to verify the accuracy of the current numerical method [28]. The geometry used in the laboratory investigation is completely consistent with that of the numerical study, with a filling ratio of 55% and having ethylene glycol as working fluid. The thermal resistance measured in the laboratory study differs from that in the current numerical study by less than 5% as shown in Fig. 7. The concordance between the simulation and experiment findings shows that the current numerical simulations can accurately represent the two-phase liquid/vapor flow in the oscillatory heat pipe. Where Q and Te represents the heat input and evaporator temperature.

Moreover, based on our current understanding, the quantity of grids exerts a somewhat indirect influence

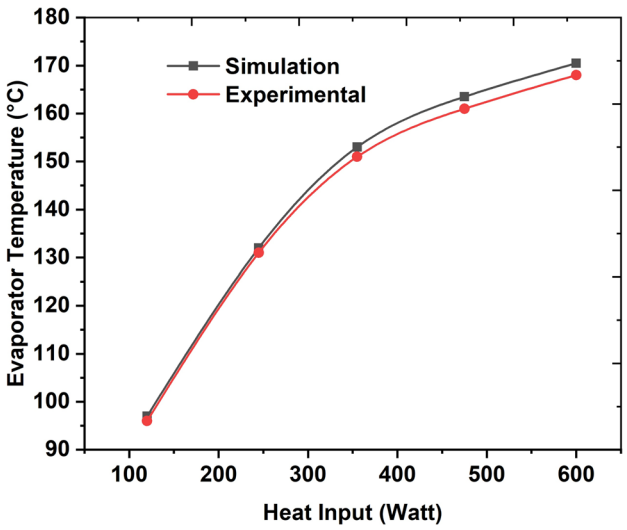

Fig. 7 Fluid temperature vs time (Evaporator and condenser) at FR (42%)

on the outcomes of numerical simulations. Four distinct grid numbers— 75,623, 55,545, 22,323 and 38,432— are employed to assess grid independence and meet the requisite criteria. Throughout the testing, all parameters remain constant, except for the grid count. When utilizing grid numbers 75623 and 55,545, as depicted in Fig. 8, the simulation results demonstrate nearly identical consistency, with a relative variance of approximately 1%. Consequently, due to the numerical precision and computational efficiency, grid number 55545 is selected for use in this study.

5.2 Effect of internal diameter

The viscous force and surface tension are directly affected by internal diameter of PHP. Where, bond no limits the

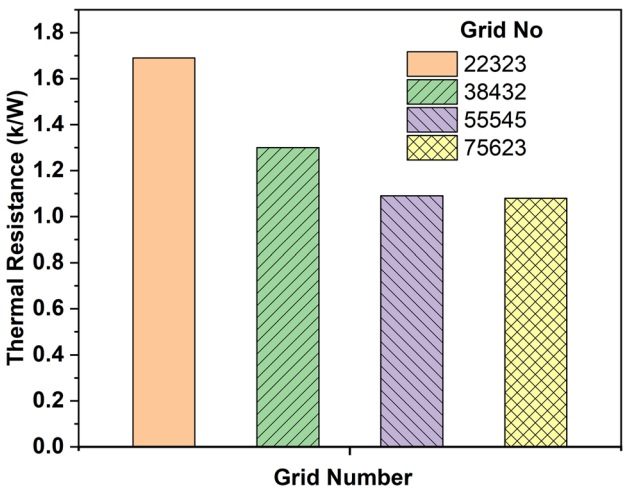

Fig. 8 Grid independence test (Q = 45 W)

maximum diameter for sustained liquid slugs [1]. The critical diameter of a pulsating heat pipe is presented in Eq. 22

$$d_{crit} = 2\sqrt{\frac{\sigma}{g(\rho_l - \rho_v)}} \tag{22}$$

The critical diameter for a pulsating heat pipe (PHP) with acetone-Al_2O_3 as the working fluid can be calculated using the eq. 2. The critical diameter comes out to be 2.1 mm. When the diameter of the PHP (Pulsating Heat Pipe) channels is smaller, the capillary forces tend to be stronger. As a result, there is an increase in liquid-vapor phase separation and the formation and growth of bubbles are promoted. This phenomenon has been distinctly observed in the PHP illustrated in the Figs. (9 and 10). When the channel diameter is closer to the critical diameter (D_{crit}), the PHP exhibits better slug-plug characteristics, leading to an improvement in overall performance. However, the minimum diameter to which a PHP can be reduced depends on several factors, including the properties of the working fluid, surface tension, fluid viscosity, channel geometry, and the desired operating conditions but there is no universal minimum diameter for a PHP [49] (Fig. 9).

Though, the figures show that the benefit of reducing the total thermal resistance, achieved by expanding the range of movement, is maintained up to a 1 mm internal diameter. The longer periods of standstill indicate a decline in surface tension forces beyond this point. The most noticeable difference is that the tiny internal diameter has more short bubbles than the large internal diameter. However, the smaller diameter leads to increased thermal resistance within the PHP, as heat transfer area decreases while the flow resistance increases as shown in Fig. 10. The rationale of above is also suggested by study [50] (Fig. 11).

It was also observed that capillary became more influential with decrease in internal diameter. A decrease in diameter enhanced capillary action due to increased surface tension effects, which may aid in overcoming gravitational forces, thus facilitating better fluid circulation. In contrast to other inner tube sizes, the lower thermal resistance value was also found for an inner diameter of 2 mm and this result is align with studies [51].

5.3 Effect of filling ratio

The transient fluid temperature variation as well as pressure drop with time in evaporator for FR 25%-75% at evaporator temperature Te = 105 K is shown in Figs. (11, 12, 13, 14, 15, 16, 17, 18, 19 and 20). It's also presumed that this filling ratio remains consistent over time. and flow is incompressible since small temperature variation. Figure 12 illustrates the T_{max} graph acquired at 0.25 FR. The oscillations observed in T_{max} over time exhibit a similar nature across various filling ratios. Yet, deviating from the norm, an intriguing trend emerges for a filling ratio of 0.55, as depicted in Fig. 13. It was observed that At a filling ratio of 25%, there exists a greater abundance of vapor plugs within the evaporator. Therefore, the time

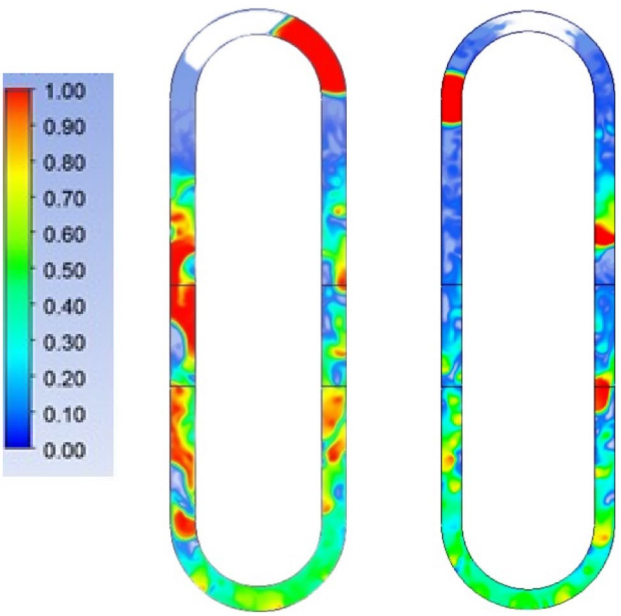

Fig. 9 Volume liquid fraction vs time value (D: 2.5 mm and 2 mm) (left to right)

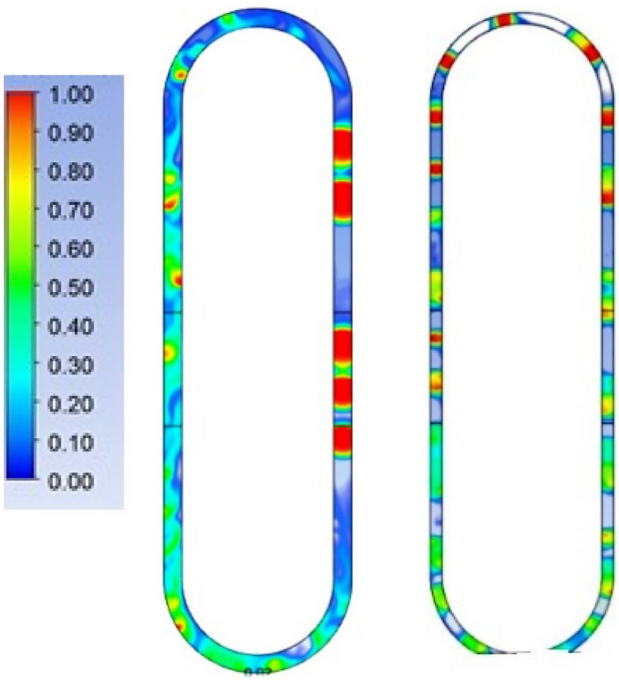

Fig. 10 Volume liquid fraction vs time value (D: 1.5 mm and 1 mm) (left to right)

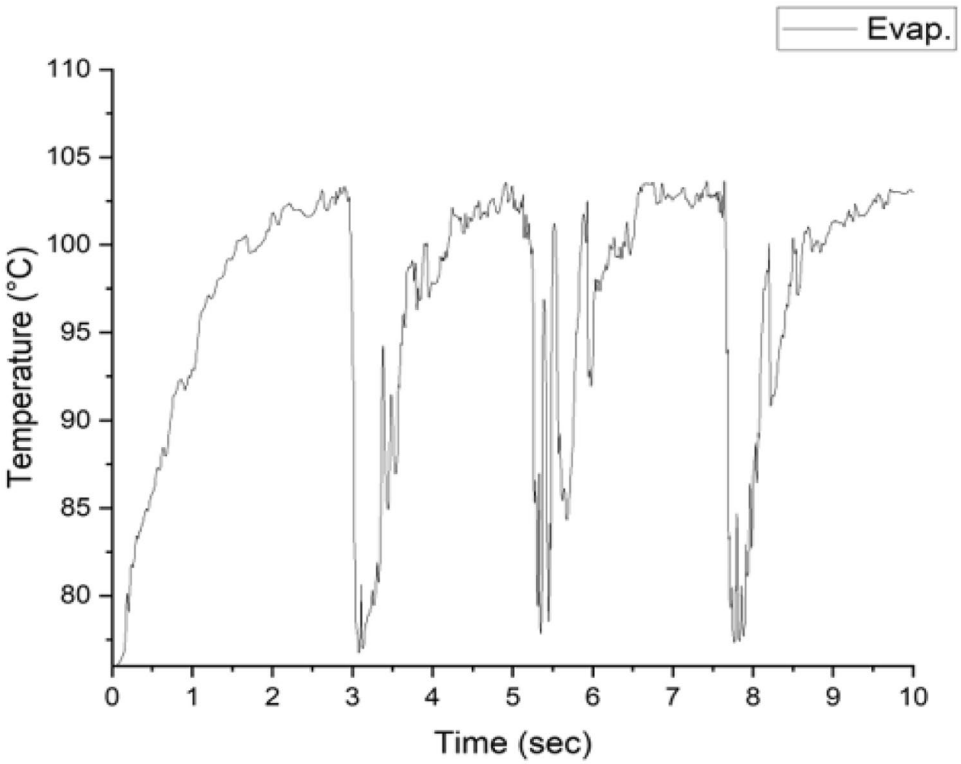

Fig. 11 Temperature Vs Time graph for Fill ratio 25%

averaged temperature of the acetone-Al_2O_3 in the evaporator section is notably elevated. In Figs. 12, 13 and 14, with the increase in filling ratio from 45 to 75%, there is a corresponding decrease in the time-averaged temperature difference of the working fluid. This phenomenon is primarily attributed to the higher.

quantity of liquid slugs presents at increased filling ratios (45% to 75%), accompanied by a higher circulation velocity of the slug flow. Since, the filling ratio determines the amount of working fluid available for heat transfer (Fig. 15).

A higher filling ratio allows for a larger amount of working fluid, resulting in higher heat transfer capability. This is because a larger volume of working fluid can absorb more heat before reaching a critical temperature [2]. It is worth to note that the temperature gradient with time decreased with increasing filling ration.

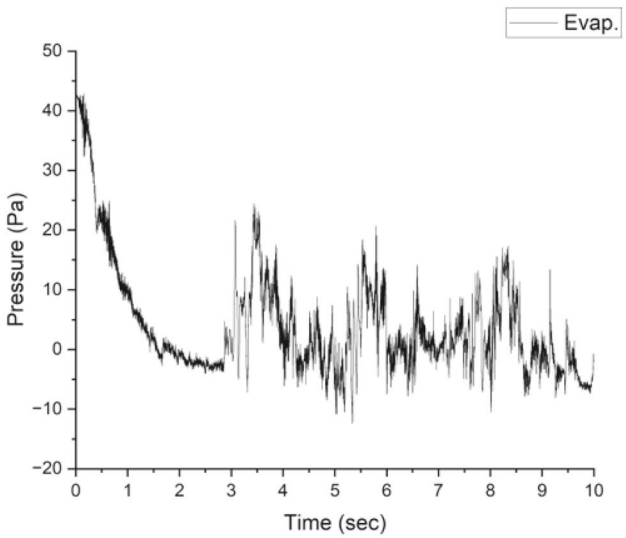

Fig. 12 Pressure vs time graph for fill ratio 25%

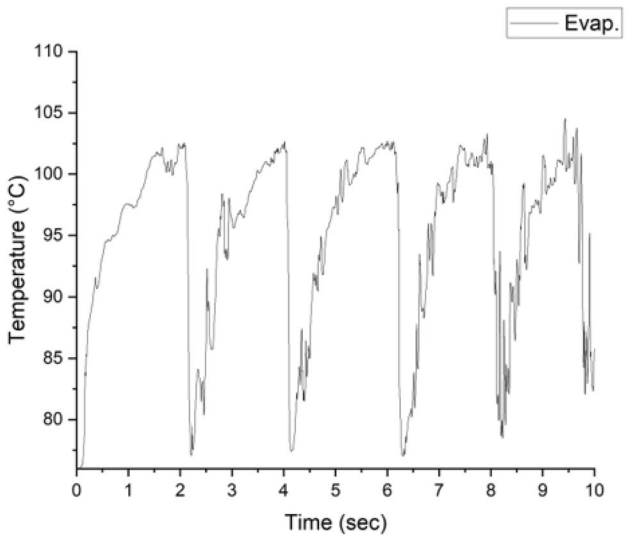

Fig. 13 Temperature vs time graph for Fill ratio 45%

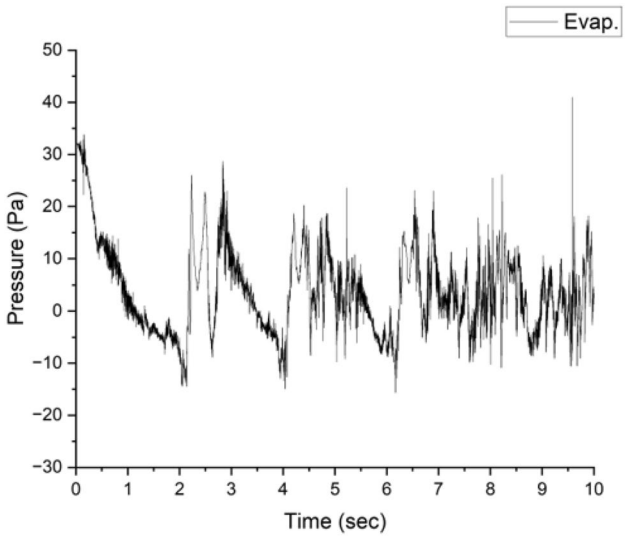

Fig. 14 Pressure vs time graph for fill ratio 45%

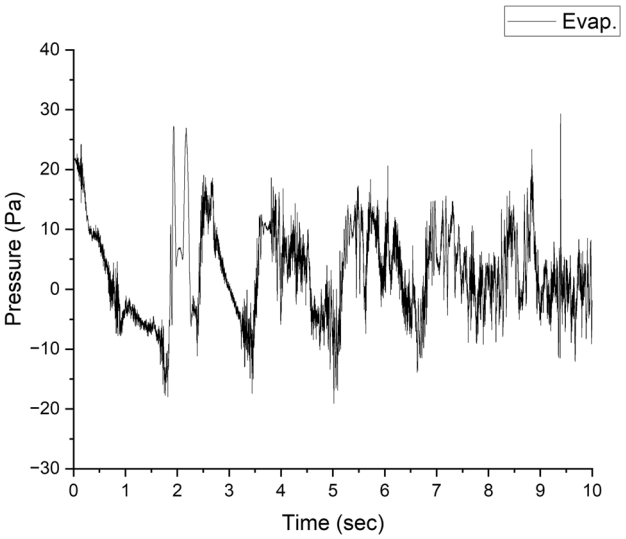

Fig. 16 Pressure vs time graph for fill ratio 55%

However, after FR = 55%, the maximum temperature also increased. At a constant filling ratio, the temperature gradient of the working fluid (the temperature difference between condenser and evaporator) rises proportionally with the improve in heat input. Nevertheless, when the filling ratio was elevated at a constant heat load, the fluid temperature gradient reduced. Hence at high heat input situation, high FR is more suitable to avoid dry out in a PHP (Fig. 16).

As the liquid content within the PHP steadily diminishes (accompanied by a corresponding increase in vapor volume), the heat transfer experiences an initial boost owing to the heightened movement of vapor plugs. Nonetheless, concurrently, the quantity of sensible heat transfer undergoes a continuous decline as a result of the diminishing liquid content. Therefore, an optimum point exists at a specific filling ratio (here, FR = 55%). The rationale of above study is also suggested by [52] Since, PHPs rely on capillary forces to transport the working fluid between the condenser and evaporator section (Fig. 17).

Capillary forces are generated by the interaction between the working fluid and the inner walls of the tube. A lower filling ratio may result in reduced capillary forces due to a smaller amount of fluid available for generating these forces [53] (Fig. 18).

Figures 12, 13 and 14 shows the pressure drop with time, and was observed that filling ratio having 75% exhibited on average highest pressure drop among all filling ratio. This is due to higher filling ratios generally lead to higher pressure

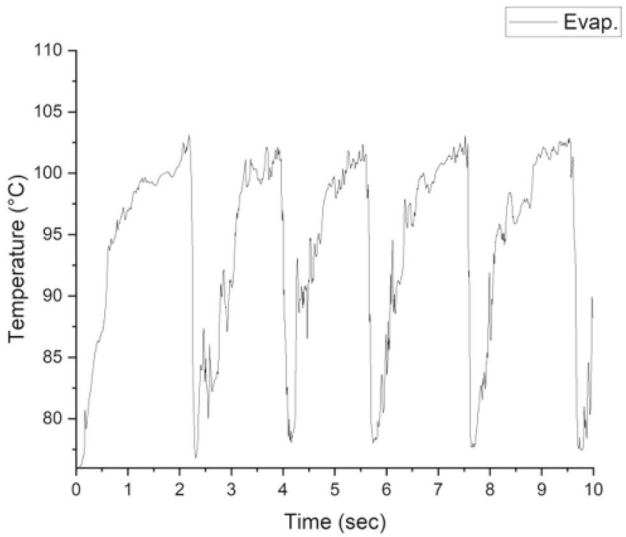

Fig. 15 Temperature vs time graph for fill ratio 55%

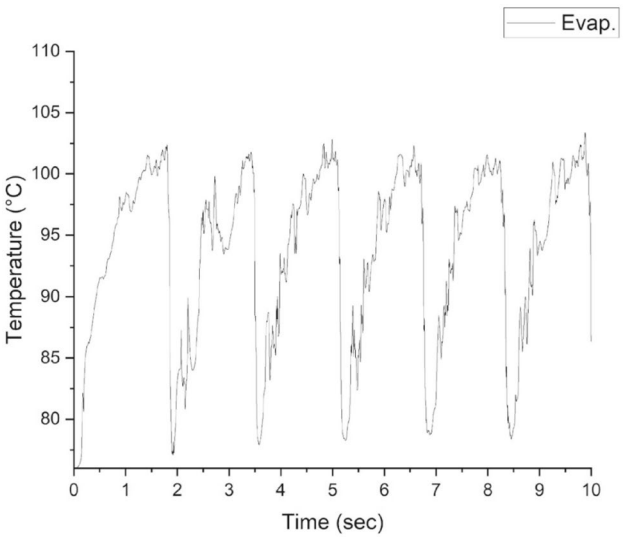

Fig. 17 Temperature vs time graph for fill ratio 65%

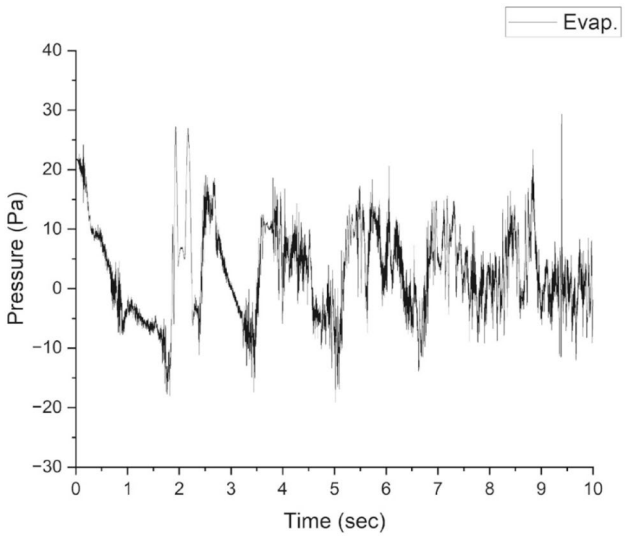

Fig. 18 Pressure vs time graph for fill ratio 65%

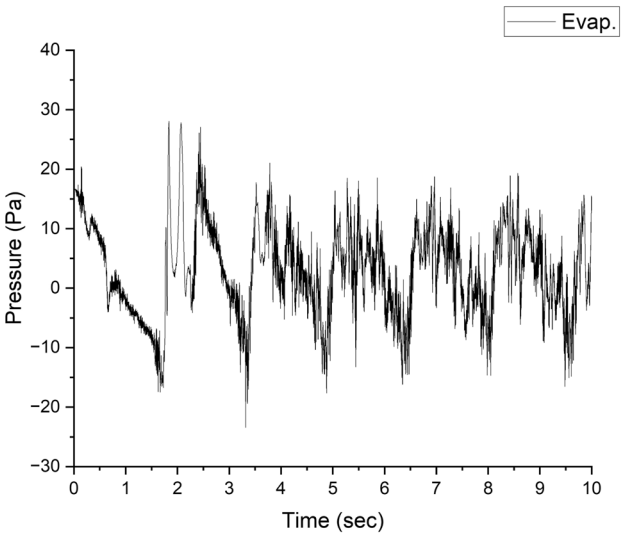

Fig. 20 Pressure vs time graph for fill ratio 75%

drops due to increased frictional resistance between the working fluid and the tube walls. This can impact the fluid flow rate and the overall system performance [54]. However, maximum pressure drop was seen for 25% filling ratio at initially small duration. It occurs due to gas entrainment: The gas plugs formed in slug flow can get entrained with the liquid slugs (Fig. 19).

As the PHP operates, these gas plugs can become dislodged from the liquid slugs, creating gas bubbles that travel through the system. The movement of gas bubbles along with the liquid slugs contributes to the overall pressure drop [55] and frictional effects: Slug flow introduces a high interfacial area between the liquid and gas phases. This increased interfacial area leads to increased frictional effects as the liquid and gas flow past each other. Frictional pressure losses occur due to the shearing forces between the two phases, resulting in additional pressure drop [56]. It is worth to note that the time averaged working fluid temperature difference (thick straight lines) evaporator decreases as FR is raised from 25 to 75%.

Additionally, there is an increased number of vapor plugs within the evaporator depicted in Fig. 20 when FR = 25%. Consequently, the time-averaged temperature of the working fluid within the evaporator section is significantly elevated as there in [57]. The time-averaged temperature differential of the working fluid decreases in Figs. 15, 16, 17, 18, 19, and 20 as FR increases from 45 to 75%. This shift is primarily attributable to the greater presence of liquid slugs at higher filling ratios (45% to 70%) and increased circulation velocities of slug flow.

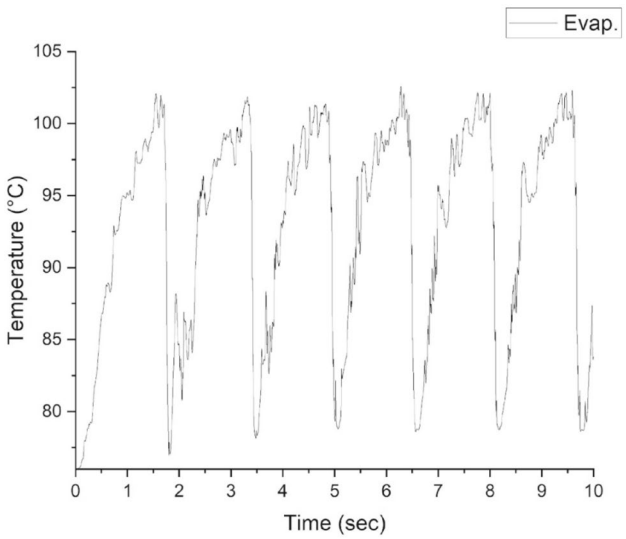

Fig. 19 Temperature vs time graph for fill ratio 75%

6 Conclusion

The pulsating heat pipe utilizing an Acetone – Al_2O_3 mixture, single turn tube, and cylindrical geometry demonstrated successful operation across various diameters and fill ratios under closed PHP valve conditions. The following conclusions are drawn from the study.

1. Increasing the diameter in a pulsating heat pipe involves a trade-off. While it can enhance heat transfer area and fluid flow dynamics, there's a limit beyond which capillary forces may become less effective. Therefore, PHP showed highest performance at 2 mm internal diameter among (1 mm, 1.5 mm, 2 mm and 2.5 mm)

2. In mixtures, the inhibition of phase transitions can significantly delay the onset of dry-out in the PHP, even when operating at low filling ratios (25%, 45%), while, Due to the reduced flow rate, the heat transmission capabilities of the PHP with acetone-Al2O3 mixtures are less effective at higher filling ratios (65 and 75%).
3. As the temperature increased, the exergy efficiency also increased linearly. However, it became nearly constant at higher temperature. Sustainability index also showed similar trends to exergy efficiency.
4. Exergy loss was lower for evaporator than condenser for a range of temperature. This is due to low temperature difference in evaporator, which can contribute to lower exergy losses.

7 Future scope

Investigate the implementation of optimal PHP configurations in real-world scenarios, considering external factors such as fluctuations in temperature. Evaluate the reliability and enduring stability of continuously operating PHP systems. Extend the investigation to explore the potential for enhancing optimization through the utilization of diverse nanoparticles and alternative working fluids. Enhance the practical applicability of PHP technology by assessing its scalability and adaptability across various industrial sectors.

Acknowledgements We would like to thank Prof. Zafar Said, University of Sharjah for key insite

Author contributions J,M,I,K,P,S: wrote the main manuscript text, prepared figures and tables P,S: reviewed the manuscript

Data availability No datasets were generated or analysed during the current study.

Declarations

Competing interests The authors declare no competing interests.

References

1. Khandekar S, Groll M (2003) On the definition of pulsating heat pipes: An overview. In Proc. 5th Minsk Int. Conf. (Heat Pipes, Heat Pumps and Refrigerators), Minsk, Belarus 707–719
2. Han X, Wang X, Zheng H, Xu X, Chen G (2016) Review of the development of pulsating heat pipe for heat dissipation. Renew Sustain Energy Rev 59:692–709
3. Rittidech S, Terdtoon P, Murakami M, Kamonpet P, Jompakdee W (2003) Correlation to predict heat transfer characteristics of a closed-end oscillating heat pipe at normal operating condition. Appl Therm Eng 23(4):497–510
4. Aminian E, Kamali M, Vatanjoo E, Saffari H (2022) Theoretical analysis on condensation heat transfer on microstructured hybrid hydrophobic-hydrophilic tube. Heat Mass Transf 58(7):1207–1221
5. Sedighi M, Ayoobi A, Aminian E (2024) Numerical investigation on forced convection enhancement within an oil cooler through the simultaneous use of porous media and nanofluid. Proceed Inst Mech Eng Part E J Proc Mech Eng 238(1):331–341
6. Zhang D, Wang L, Xu B, Li Q, Wang S, An Z (2024) Experimental and simulation study on flow heat transfer characteristics of flat pulsating heat pipe with wide and narrow interphase channels. Appl Therm Eng 122806
7. Zhang D, He Z, Jiang E, Shen C, Zhou J (2021) A review on start-up characteristics of the pulsating heat pipe. Heat Mass Transf 57:723–735
8. Pachghare PR, Mahalle AM (2014) Thermo-hydrodynamics of closed loop pulsating heat pipe: An experimental study. J Mech Sci Technol 28:3387–3394
9. Zhang D, He Z, Guan J, Tang S, Shen C (2022) Heat transfer and flow visualization of pulsating heat pipe with silica nanofluid: An experimental study. Int J Heat Mass Transf 183:122100
10. Faghri A (2012) Review and advances in heat pipe science and technology. J Heat Transfer 134(12):123001
11. Markal B, Aksoy K (2021) The combined effects of filling ratio and inclination angle on thermal performance of a closed loop pulsating heat pipe. Heat Mass Transf 57:751–763
12. Talesh Bahrami HR, Aminian E, Saffari H (2020) Energy transfer enhancement inside an annulus using gradient porous ribs and nanofluids. J Energy Res Technol 142(12):122102
13. Arab M, Soltanieh M, Shafii MB (2012) Experimental investigation of extra-long pulsating heat pipe application in solar water heaters. Exp Thermal Fluid Sci 42:6–15
14. Qu W, Yang B 2009 Performances of flat plate pulsating heat pipes. In International Conference on Micro/Nanoscale Heat Transfer 43918:403–410
15. Aminian E, Saffari H (2022) Experimental analysis of dropwise condensation heat transfer on a finned tube: Impact of pitch size. Proceed Inst Mech Eng Part A J Power Energy 236(4):752–759
16. Liang Q, Li Y, Wang Q (2018) Effects of filling ratio and condenser temperature on the thermal performance of a neon cryogenic oscillating heat pipe. Cryogenics 89:102–106
17. Zhang XM (2004) Experimental study of a pulsating heat pipe using FC-72, ethanol, and water as working fluids. Experimental Heat Transfer 17(1):47–67
18. Saha M, Feroz CM, Ahmed F, Mujib T (2012) Thermal performance of an open loop closed end pulsating heat pipe. Heat Mass Transf 48:259–265
19. Siavashi M, Bahrami HT, Aminian E, Saffari H (2019) Numerical analysis on forced convection enhancement in an annulus using porous ribs and nanoparticle addition to base fluid. J Central South Univ 26(5):1089–1098
20. Smrity AMA, Yin P (2024) Design and performance evaluation of pulsating heat pipe using metallic nanoparticles based hybrid nanofluids. Int J Heat Mass Transf 218:124773
21. Babaei A, Aminian E, Saffari H (2023) Numerical study of heat transfer and pressure drop of nanofluids in a combined porous media of hydrophobic and hydrophilic surfaces. Proceed Inst Mech Eng Part A J Power Energy 237(6):1308–1328
22. Karthikeyan VK, Ramachandran K, Pillai BC, Solomon AB (2014) Effect of nanofluids on thermal performance of closed loop pulsating heat pipe. Exp Thermal Fluid Sci 54:171–178
23. Ji Y, Ma H, Su F, Wang G (2011) Particle size effect on heat transfer performance in an oscillating heat pipe. Exp Thermal Fluid Sci 35(4):724–727
24. Tanshen MR, Munkhbayar B, Nine MJ, Chung H, Jeong H (2013) Effect of functionalized MWCNTs/water nanofluids on thermal resistance and pressure fluctuation characteristics in oscillating heat pipe. Int Commun Heat Mass Transfer 48:93–98

25. Bhuwakietkumjohn N, Rittidech S (2010) Internal flow patterns on heat transfer characteristics of a closed-loop oscillating heat-pipe with check valves using ethanol and a silver nano-ethanol mixture. Exp Thermal Fluid Sci 34(8):1000–1007
26. Qu J, Wu H (2011) Thermal performance comparison of oscillating heat pipes with SiO2/water and Al_2O_3/water nanofluids. Int J Therm Sci 50(10):1954–1962
27. Jouhara H, Khordehgah N, Almahmoud S, Delpech B, Chauhan A, Tassou SA (2018) Waste heat recovery technologies and applications. Therm Sci Eng Prog 6:268–289
28. Rudresha S, Babu ER, Thejaraju R (2023) Experimental investigation and influence of filling ratio on heat transfer performance of a pulsating heat pipe. Therm Sci Eng Prog 38:101649
29. White ET, Beardmore RH (1962) The velocity of rise of single cylindrical air bubbles through liquids contained in vertical tubes. Chem Eng Sci 17(5):351–361
30. Khandekar S (2004) Thermo-hydrodynamics of closed loop pulsating heat pipes
31. Mameli M, Manno V, Filippeschi S, Marengo M (2014) Thermal instability of a closed loop pulsating heat pipe: Combined effect of orientation and filling ratio. Exp Thermal Fluid Sci 59:222–229
32. Vatanjoo E, Aminian E, Kamali M, Saffari H (2023) Theoretical analysis on condensation heat transfer on the hydrophobic–hydrophilic hybrid surfaces with the impact of the Marangoni convection. Proceed Inst Mech Eng Part E J Process Mech Eng 237(3):658–672
33. Wang W, Cui X, Zhu Y (2017) Heat transfer performance of a pulsating heat pipe charged with acetone-based mixtures. Heat Mass Transf 53:1983–1994
34. Mameli M, Mangini D, Vanoli GFT, Araneo L, Filippeschi S, Marengo M (2016) Advanced multi-evaporator loop thermosyphon. Energy 112:562–573
35. Mameli M, Marengo M, Khandekar S (2014) Local heat transfer measurement and thermo-fluid characterization of a pulsating heat pipe. Int J Therm Sci 75:140–152
36. Holman JP (2001) Experimental methods for engineers
37. Yadav PS, Said Z, Gautam R, Raman R, Caliskan H (2023) Novel investigation on atomization, performance, and emission characteristics of preheated jatropha oil methyl ester and ethyl ester. Energy 270:126870
38. Rashidi MM, Mahariq I, Alhuyi Nazari M, Accouche O, Bhatti MM (2022) Comprehensive review on exergy analysis of shell and tube heat exchangers. J Therm Anal Calorim 147(22):12301–12311
39. Dincer I, Rosen MA (2012) Exergy: Energy, environment and sustainable development. Newnes
40. Bejan A, Tsatsaronis G, Moran MJ (1995) Thermal design and optimization. John Wiley & Sons
41. Rosen MA, Dincer I, Kanoglu M (2008) Role of exergy in increasing efficiency and sustainability and reducing environmental impact. Energy Policy 36(1):128–137
42. Pastukhov VG, Maydanik YF (2016) Development of a pulsating heat pipe with a directional circulation of a working fluid. Appl Therm Eng 109:155–161
43. Karthikeyan VK, Ramachandran K, Pillai BC, Brusly Solomon A (2015) Understanding thermo-fluidic characteristics of a glass tube closed loop pulsating heat pipe: Flow patterns and fluid oscillations. Heat Mass Transf 51:1669–1680
44. Wang J, Xie J, Liu X (2020) Investigation of wettability on performance of pulsating heat pipe. Int J Heat Mass Transf 150:119354
45. Lin Z, Wang S, Shirakashi R, Zhang LW (2013) Simulation of a miniature oscillating heat pipe in bottom heating mode using CFD with unsteady modeling. Int J Heat Mass Transf 57(2):642–656
46. Minko KB, Artemov VI, Klementiev AA (2024) CFD simulation of the inundation effect for saturated propane vapor condensation on the surface of a horizontal tube using the volume of fluid method. Int Commun Heat Mass Transfer 154:107432
47. Aminian E, Moghadasi H, Saffari H (2020) Magnetic field effects on forced convection flow of a hybrid nanofluid in a cylinder filled with porous media: A numerical study. J Therm Anal Calorim 141:2019–2031
48. Liu Y, Dan D, Wei M, Zheng S, Sun J (2024) Numerical investigation on the start-up and heat transfer performance of dual-diameter pulsating heat pipes. Appl Therm Eng 236:121709
49. Li Z, Sarafraz MM, Mazinani A, Moria H, Tlili I, Alkanhal TA, . . . Safaei MR (2020) Operation analysis, response and performance evaluation of a pulsating heat pipe for low temperature heat recovery. Energy Convers Manag 222:113230
50. Wang J, Pan Y, Liu X (2021) Investigation on start-up and thermal performance of the single-loop pulsating heat pipe with variable diameter. Int J Heat Mass Transf 180:121811
51. Babu ER, Reddy NC, Babbar A, Chandrashekar A, Kumar R, Bains PS, . . . Ammarullah MI (2024) Characteristics of pulsating heat pipe with variation of tube diameter, filling ratio, and SiO2 nanoparticles: Biomedical and engineering implications. Case Stud Therm Eng 55:104065
52. Jajarm ARA, Goshayeshi HR, Bashirnezhad K, Chaer I, Toghraie D, Salahshour S (2024) Combined effect of the magnetic field, orientation, and filling ratio on cylindrical pulsating heat pipe using distilled water and distilled water/Fe3O4 nanofluid. J Magn Magn Mater 590:171712
53. Spinato G, Borhani N, Thome JR (2015) Understanding the self-sustained oscillating two-phase flow motion in a closed loop pulsating heat pipe. Energy 90:889–899
54. Chen X, Lin Y, Shao S, Wu W (2019) Study on heat transfer characteristics of ethane pulsating heat pipe in middle-low temperature region. Appl Therm Eng 152:697–705
55. Rittidech S, Donmaung A, Kumsombut K (2009) Experimental study of the performance of a circular tube solar collector with closed-loop oscillating heat-pipe with check valve (CLOHP/CV). Renew Energy 34(10):2234–2238
56. Zolfaghari A, Aminian E, Saffari H (2022) Numerical investigation on entropy generation in the dropwise condensation inside an inclined pipe. Heat Transfer 51(1):551–577
57. Barua H, Ali M, Nuruzzaman M, Islam MQ, Feroz CM (2013) Effect of filling ratio on heat transfer characteristics and performance of a closed loop pulsating heat pipe. Proc Eng 56:88–95

Terms and Conditions

Springer Nature journal content, brought to you courtesy of Springer Nature Customer Service Center GmbH (“Springer Nature”).
Springer Nature supports a reasonable amount of sharing of research papers by authors, subscribers and authorised users (“Users”), for small-scale personal, non-commercial use provided that all copyright, trade and service marks and other proprietary notices are maintained. By accessing, sharing, receiving or otherwise using the Springer Nature journal content you agree to these terms of use (“Terms”). For these purposes, Springer Nature considers academic use (by researchers and students) to be non-commercial.
These Terms are supplementary and will apply in addition to any applicable website terms and conditions, a relevant site licence or a personal subscription. These Terms will prevail over any conflict or ambiguity with regards to the relevant terms, a site licence or a personal subscription (to the extent of the conflict or ambiguity only). For Creative Commons-licensed articles, the terms of the Creative Commons license used will apply.
We collect and use personal data to provide access to the Springer Nature journal content. We may also use these personal data internally within ResearchGate and Springer Nature and as agreed share it, in an anonymised way, for purposes of tracking, analysis and reporting. We will not otherwise disclose your personal data outside the ResearchGate or the Springer Nature group of companies unless we have your permission as detailed in the Privacy Policy.
While Users may use the Springer Nature journal content for small scale, personal non-commercial use, it is important to note that Users may not:

1. use such content for the purpose of providing other users with access on a regular or large scale basis or as a means to circumvent access control;
2. use such content where to do so would be considered a criminal or statutory offence in any jurisdiction, or gives rise to civil liability, or is otherwise unlawful;
3. falsely or misleadingly imply or suggest endorsement, approval , sponsorship, or association unless explicitly agreed to by Springer Nature in writing;
4. use bots or other automated methods to access the content or redirect messages
5. override any security feature or exclusionary protocol; or
6. share the content in order to create substitute for Springer Nature products or services or a systematic database of Springer Nature journal content.

In line with the restriction against commercial use, Springer Nature does not permit the creation of a product or service that creates revenue, royalties, rent or income from our content or its inclusion as part of a paid for service or for other commercial gain. Springer Nature journal content cannot be used for inter-library loans and librarians may not upload Springer Nature journal content on a large scale into their, or any other, institutional repository.
These terms of use are reviewed regularly and may be amended at any time. Springer Nature is not obligated to publish any information or content on this website and may remove it or features or functionality at our sole discretion, at any time with or without notice. Springer Nature may revoke this licence to you at any time and remove access to any copies of the Springer Nature journal content which have been saved.
To the fullest extent permitted by law, Springer Nature makes no warranties, representations or guarantees to Users, either express or implied with respect to the Springer nature journal content and all parties disclaim and waive any implied warranties or warranties imposed by law, including merchantability or fitness for any particular purpose.
Please note that these rights do not automatically extend to content, data or other material published by Springer Nature that may be licensed from third parties.
If you would like to use or distribute our Springer Nature journal content to a wider audience or on a regular basis or in any other manner not expressly permitted by these Terms, please contact Springer Nature at

onlineservice@springernature.com